Deep-Sea Research, Vol. 39, No. 6, pp. 997–1014, 1992.
Printed in Great Britain.

0198–0149/92 $5.00 + 0.00
© 1992 Pergamon Press Ltd

Annual cycle of the Atlantic North Equatorial Countercurrent

PHILIP L. RICHARDSON,* SABINE ARNAULT,† SILVIA GARZOLI‡
and JOHN G. BRUCE§

(*Received* 30 *July* 1991; *in revised form* 2 *October* 1991; *accepted* 2 *October* 1991)

Abstract—An analysis of numerous meridional XBT sections near 28°W reveals that the geostrophic North Equatorial Countercurrent (NECC) continues to flow eastward throughout the year, fastest in fall and slowest in spring. Drifting buoys and historical ship drifts show that the near-surface Countercurrent reverses each spring even when systematic errors due to windage are taken into account. The seasonally fluctuating winds drive an Ekman surface current that is eastward in fall, adding to the geostrophic current, and westward in spring, countering and overwhelming the geostrophic current. The reversal of the Countercurrent in spring occurs in the near-surface layer and is driven by the Northeast Trades. Thus the near-surface velocity in the Countercurrent is determined by a competition between local wind stress and the larger field of wind stress curl, both of which have large seasonal variations in the tropical Atlantic.

1. INTRODUCTION

THE North Equatorial Countercurrent (NECC) flows eastward across the tropical Atlantic, sandwiched between the westward flowing South Equatorial Current (SEC) and North Equatorial Current (NEC) (Fig. 1). The Countercurrent plays a vital role in modulating meridional water and heat flux through the Tropical Atlantic (PHILANDER and PACANOWSKI, 1986). Yet our knowledge of this current is really quite fragmentary. The best data set of direct velocity is from the near-surface layer; the subsurface velocity field has been inferred mainly from a few meridional hydrographic sections, a meridional array of inverted echo sounders and a single current meter mooring at 6°N, 28°W.

Drifting buoys have revealed that the near-surface NECC reverses each spring west of about 20°W (RICHARDSON and REVERDIN, 1987). This finding agrees with historical ship drifts (ARNAULT, 1987; RICHARDSON and REVERDIN, 1987) and a study of historical temperature data (GARZOLI and KATZ, 1983). However, other studies using hydrographic and conductivity–temperature–depth (CTD) data have concluded that the geostrophic NECC continues eastward throughout the year although it is weaker in spring (COCHRANE *et al.*, 1979; MERLE and ARNAULT, 1985; ARNAULT, 1987; HENIN and HISARD, 1987). Most

*Department of Physical Oceanography, Woods Hole Oceanographic Institution, Woods Hole, MA 02543, U.S.A.
†Laboratoire d'Océanographie Dynamique et de Climatologie, Université Pierre and Marie Curie, 75252 Paris Cedex 05, France.
‡Lamont–Doherty Geological Observatory of Columbia University, Palisades, NY 10964, U.S.A.
§Ocean Technology Branch, U.S. Naval Oceanographic Office, Stennis Space Center, MS 39522, U.S.A.

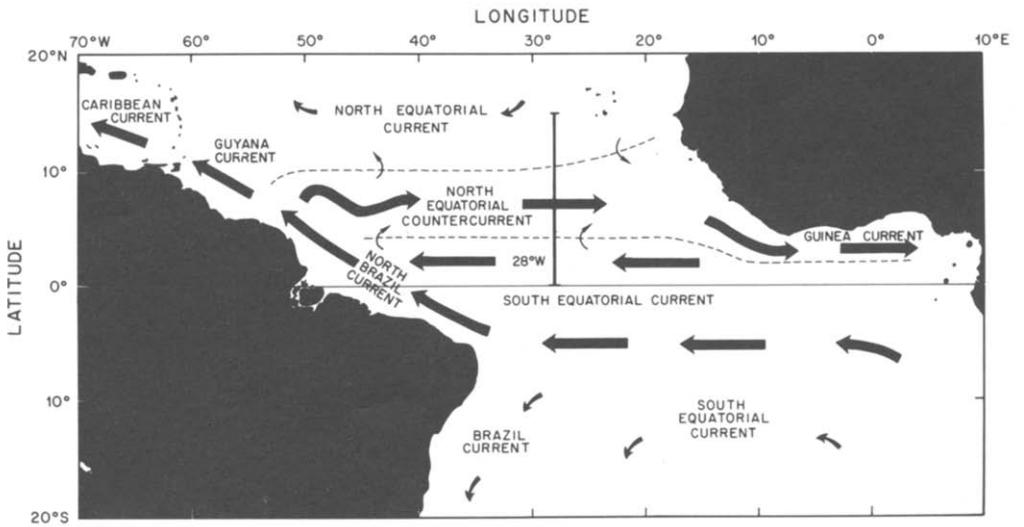

Fig. 1. Schematic diagram of surface currents in the tropical Atlantic between July and September, when the NECC flows swiftly eastward across the Atlantic. From January to June (approximately) the NECC disappears, and westward surface velocities are seen in this area. Thick arrows represent currents greater than 30 cm s^{-1}. The line along 28°W shows the region of the present study.

hydrographic sections across the NECC in spring reveal what looks like a nearly flat large-scale field of dynamic height, with superposed significant mesoscale fluctuations that could be interpreted as eddies or current jets. It is difficult to know whether these sections show a permanent current or merely higher frequency fluctuations (or both). Thus the interpretation of the historical hydrographic data is problematic, especially for the spring.

Time series of estimated surface dynamic height have been obtained with inverted echo sounders across the NECC (3° and 9°N) over 20 months (KATZ, 1987; GARZOLI and RICHARDSON, 1989). The sounders along 38°W suggest that the NECC reverses seasonally, but those along 28°W imply the NECC flow is near zero in spring. The sounders along 28°W also suggest a long period meandering of the NECC related to latitudinal shifts of the intertropical convergence zone (GARZOLI and RICHARDSON, 1989). Inferring geostrophic velocity in spring is made difficult because of the large amplitude higher-frequency oscillations, eddies and the meandering of the NECC, and the large meridional spacing between instruments that could cause spatial aliasing (RICHARDSON and REVERDIN, 1987; GARZOLI and RICHARDSON, 1989).

The only continuous, long term, subsurface velocity measurements in the NECC are from a single current meter mooring near the center of the NECC at 6°N, 28°W (RICHARDSON and REVERDIN, 1987). These velocity series at 20–300 m show that the eastward flow weakens and possibly reverses in spring. However, large-amplitude fluctuations with a period of around a month make it difficult to see clearly the annual period fluctuation. Inferring characteristics of a complicated current that varies in width (HENIN and HISARD, 1987) and latitude (GARZOLI and RICHARDSON, 1989) throughout the year

from a single mooring site is clearly problematic. Thus the evidence for a seasonally reversing NECC is incomplete and contradictory.

ARNAULT (1987) shed light on the question of the NECC reversal by using historical data to study surface velocity in the tropical Atlantic. She found that when the near-surface Ekman current (calculated with climatological winds) was added to the surface geostrophic current (calculated with historical hydrographic casts), the sum was very nearly equal to the velocity measured with historical ship drifts. The geostrophic NECC continued eastward year around, yet the combined surface velocity was westward in spring, due to the Ekman velocity. The work described here expands on Arnault's analysis by using newer, more numerous, and higher resolution data across the NECC. The new data are expendable bathythermographs (XBTs) taken from ships of opportunity which traversed the NECC near 28°W. These sections, made during 1980–1985, provide many times the amount of data previously available.

We use these data to calculate an average seasonal cycle of eastward geostrophic velocity in the vicinity of the NECC (from 1° to 15°N), add it to the eastward Ekman current, and compare results to velocity measured directly with ship drifts and drifting buoys. The sum of Ekman and geostrophic velocity is found to agree closely with the direct observations, as was found by Arnault. We explore reasons why this might be so based on how we calculate Ekman velocity, and we compare simulations of Ekman velocity calculated with a numerical model. Finally, direct velocity measurements made in the NECC are used to examine the wind driven shear within the upper 50 m and a systematic downwind measurement bias is estimated.

2. DATA AND METHODS

2.1. *XBT sections*

During the SEQUAL (Seasonal Response of the Equatorial Atlantic) and FOCAL (Français Ocean et Climat dans l'Atlantique Equatorial) programs, numerous nearly meridional XBT sections were made across the NECC near 28°W (Fig. 2, see HEIMERDINGER, 1987). They consist of:

(1) SEQUAL ship-of-opportunity sections, a NW–SE line along which XBTs were taken every 1/3 degree in latitude from 0° to 10°N (BRUCE, 1987);

(2) FOCAL and German ship-of-opportunity sections, a NE–SW line along which XBTs were taken every few degrees (RUAL and JARRIGE, 1984; HEIMERDINGER, 1987; EMERY *et al.*, 1987; REVERDIN *et al.*, 1991); and

(3) four sections along 28°W made during SEQUAL mooring cruises (MELE and KATZ, 1985) plus a CTD section by PERKINS and SAUNDERS (1984).

The data consist of approximately 1400 individual temperature profiles to 440 m spread rather evenly over the years 1980–1985. On average there are nearly eight observations per degree latitude each month in the latitudinal band 0°–15°N. The FOCAL and German sections are discussed by EMERY *et al.* (1987) who plotted time series of dynamic height and geostrophic velocity relative to 300 m, and a longer series is described by REVERDIN *et al.* (1991) who investigate the annual variability of temperature and currents.

We plotted each XBT profile, and compared it visually to its neighbors, and discarded obviously erroneous ones and any that did not reach 440 m. Using a shallower depth would have yielded more data but would have missed variations in deeper temperature. We will

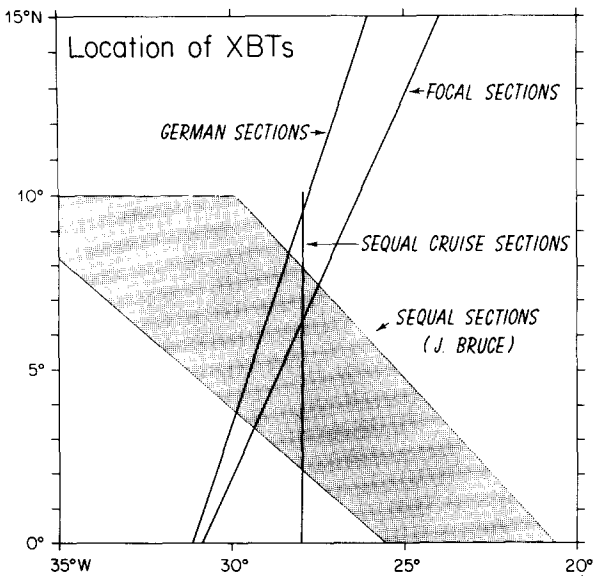

Fig. 2. Location of the XBT sections analysed in this paper.

discuss later the effect of geostrophic shear below 400 m. Each remaining temperature profile was subsampled to obtain values at 20 m levels.

2.2. *Salinity*

Salinities were estimated at 20 m depth intervals from mean T–S curves for each 2° latitude band bounded by longitudes 24°–32°W. The mean T–S curves were calculated using historical hydrographic measurements from 1900 to 1978 (ARNAULT, 1987). Variations of the T–S relation were noticeable in the upper 75–100 m, but the available data were insufficient to resolve adequately the mean seasonable variations as a function of latitude. The omission of this variation leads to errors in dynamic height and geostrophic velocity, but these are much smaller than the dominant seasonal variations caused by vertical heaving of the thermocline.

2.3. *Dynamic height*

Density and dynamic height (relative to 440 m) were calculated for each profile of temperature and estimated salinity. Individual values of dynamic height at the sea surface were plotted on a time–latitude diagram and obviously erroneous values discarded. Large data gaps occur for some months and years, which implied the data were too sparse to resolve the meridional structure of the seasonal variations accurately during each of the six years. Therefore all observations were grouped into 1° latitude by 1 month bins and an average seasonal variation of velocity was calculated. The resulting latitude–month series was smoothed so that an individual anomalous value relative to the background field was reduced by 83%, with 60% of the reduction applied to the eight nearest neighbors. The

resulting distribution kept all the large scale features of the unsmoothed series but reduced noise that would have been amplified in calculating geostrophic velocity.

The error due to using the mean T–S relation vs the seasonally varying T–S relation was estimated by calculating dynamic height from CTD data located between 4°–6°N and 24°–32°W. Monthly dynamic height values relative to 400 db were calculated two ways; first for CTD temperature profiles using the historical mean T–S relation and second using the CTD T and S profiles. The mean difference of the two techniques is around 0.5 dynamic cm (dyn cm), with largest differences around 1.0 dyn cm occurring in the winter season and near zero differences during the rest of the year. These values are small compared to the mean seasonal variation at this location which is around 10 dyn cm. The averaged dynamic height variation across the NECC varies from around 20 dyn cm in October to around 5 dyn cm in April. The estimated error of 1 dyn cm becomes relatively larger in spring but not so large as to qualitatively change the seasonal variations discussed below.

Near the equator and also at 10°N, the XBT lines are spread out in longitude (Fig. 2). This could have caused problems if there were significant zonal variations in dynamic height. To evaluate this potential problem we calculated two seasonal time series of dynamic height by grouping (a) the SEQUAL sections and (b) the FOCAL and German sections. Comparison showed no systematic difference between the two series, implying that the dominant fluctuations are meridional, not zonal, and that the geostrophic currents are primarily zonal, not meridional. Because the XBT lines converge near the center of the NECC near 4°–7°N, these latitudes should be the least biased by any unresolved zonal variations in dynamic height.

2.4. *Geostrophic velocity*

Zonal baroclinic geostrophic velocity relative to 440 db was calculated for each month from the 1° averaged dynamic height values. Meridional gradients of dynamic height across 1° latitude bands were multiplied by $1/f\Delta x$, where f is the Coriolis parameter and Δx is 1° in latitude. Close to the equator, $f \rightarrow 0$ and dynamic height gradients are highly amplified. This should be kept in mind when viewing the large amplitudes of geostrophic velocity obtained at 1° and 2°N.

The error in surface velocity caused by the neglect of seasonal variations in T–S is estimated by assuming a 1 dyn cm error across the 8° width of the NECC, which amounts to an error in velocity of around 1 cm s^{-1}. This assumes that the latitudinal variations in the seasonality in T–S relation are dominant at the scale of the major currents. If the latitudinal variations of the seasonal T–S relation occur on smaller scales, then the error in surface velocity could be larger than 1 cm s^{-1}.

Potentially more significant is the baroclinic shear below 440 db, the assumed reference level used here. To estimate this error we studied a set of historical CTD stations that extended to at least 1000 m. Pairs of stations were selected and geostrophic velocity profiles were calculated based on the following criteria. The pairs of stations were located in the 0°–10°N band near the same longitude, were sampled on the same day, and contained reasonable looking T–S profiles. Forty-six stations resulted in 23 velocity profiles. The surface velocity was calculated using reference levels at 400 and 1000 m. The average surface zonal speed referenced to 400 m is 23.5 cm s^{-1} and to 1000 m is 23.3 cm s^{-1}, indicating that on average there is little mean shear between 400 and 1000 m. Individual profiles differ significantly from this mean, however. Restricting ourselves to the 10

velocity profiles in the vicinity of the NECC (5°–10°N, 20°–40°W) during spring, when the currents are weak (there were few station pairs in other seasons), the average surface speed referenced to 400 m is 10.7 cm s^{-1} and to 1000 m is 11.9 cm s^{-1}. Thus the average zonal speed at 400 m relative to 1000 m is 1.2 cm s^{-1}. This is somewhat smaller than the standard error, ± 1.9 cm s^{-1}, of the 10 values of zonal speed at 400 m relative to 1000 m. These data from the NECC suggest that the mean shear between 1000 and 400 m is in the same direction as that between 400 m and the surface (although individual profiles differ significantly from the mean) and that the mean deeper shear is roughly 10% of the upper layer shear, although the mean deep shear is smaller than the estimated standard error. Our conclusion is that the baroclinic geostrophic surface velocity referenced to 440 m is a fairly good representation of that referenced to 1000 m, but the deep data are not sufficiently dense to tell how good. [REVERDIN *et al.* (1991) also discuss the accuracy and representativeness of the XBT data.] Since even fairly weak deep shear is important when used to calculate geostrophic volume transport, the transport of the NECC referenced to 400 m is subject to a higher relative uncertainty than the surface velocity.

2.5. *Ship drifts and drifters*

A major ship route containing numerous historical ship drift velocities closely follows the FOCAL and German XBT lines (Fig. 2). Along this line the data density is approximately 500 observations per 1° square. Individual historical ship drifts along this line and lying between 23° and 33°W were grouped into bins 1° in latitude and 1 month in time, and averaged zonal velocity was calculated for all years combined.

Many possible random and systematic errors can occur during ship drift measurements, and it is difficult with available information to evaluate the errors very accurately. Ship drift measurements and errors have been discussed by RICHARDSON and MCKEE (1984), RICHARDSON and WALSH (1986) and MCPHADEN *et al.* (1991). A single velocity measurement is estimated from a consideration of errors in position fixes and dead reckoning to have a random error of ~20 cm s^{-1}. When large numbers of observations are available, as they are along the main ship track, the standard error of the calculated mean velocity is relatively small. On average, the monthly 1° bins contained 250 individual observations. This reduces the standard error to around 1.3 cm s^{-1}, small compared to the seasonal variations of currents. A larger concern is the possible systematic error caused by wind and wave forces on the ships which could cause the ships to slip through the water in the downwind direction. Because of the complexity of the problem and lack of data with which to calibrate ship drift velocities, the size of this error has remained unknown. We will return to this problem later.

Velocity values measured by drogued drifting buoys during SEQUAL and FOCAL (RICHARDSON and REVERDIN, 1987) were similarly grouped in bins 2° in latitude and 2 months. Larger bins were used than for ship drifts because of a lower drifter data density and to reduce the size of the standard errors. In the vicinity of the NECC the typical bin contained 125 daily drifter observations. The standard error was estimated to be ~10 cm s^{-1} from $\sqrt{2T\sigma/N}$, where T is the integral time scale of the autocorrelation function (22 days), N is the number of daily velocity observations (125), and σ the variance of eastward velocity (~300 cm^2 s^{-2}).

A window-shade-style drogue was attached to the drifters, centered at a depth of 20 m; the ratio of the drag of the drogue to the tether and surface buoy is estimated to be 16 to 1.

The average downwind drifter velocity relative to that measured by a current meter at 20 m is estimated to be 4.5 cm s^{-1} ± 0.7 cm s^{-1}. This velocity, which is interpreted to be slippage due to winds and current shear, will be discussed more fully later.

2.6. *Ekman surface current*

The wind-driven surface current was calculated by ARNAULT (1987) from the Ekman relationship and climatological monthly average wind stress (HELLERMAN and ROSENSTEIN, 1983). Values from 26° to 30°W were averaged in 2° latitude bins and interpolated linearly at each degree of latitude. Surface velocity was assumed to be 45° to the right of the wind and equal in magnitude to $V_0 = \tau/[\rho(fA_z)^{1/2}]$, where τ is the wind stress, f is the Coriolis parameter, ρ is density, and A_z is the vertical viscosity, assumed to be equal to 10^2 cm^2 s^{-1} (ARNAULT, 1987). This value of A_z was found by Arnault to be appropriate in various current regimes in the tropical Atlantic, including the NECC. We verified that these values were appropriate for our region by plotting Ekman velocity against the difference between ship drift and baroclinic geostrophic velocity (Fig. 3). The data lie close to a one to one relationship. Using classical Ekman theory to calculate wind-driven surface current is admittedly rather simple, but it has been found to be in good agreement with current and wind measurements (HALPERN, 1979). Clearly, however, the Ekman surface drift velocity is merely a crude approximation of what occurs in the real ocean driven by variable winds and buoyancy fluxes.

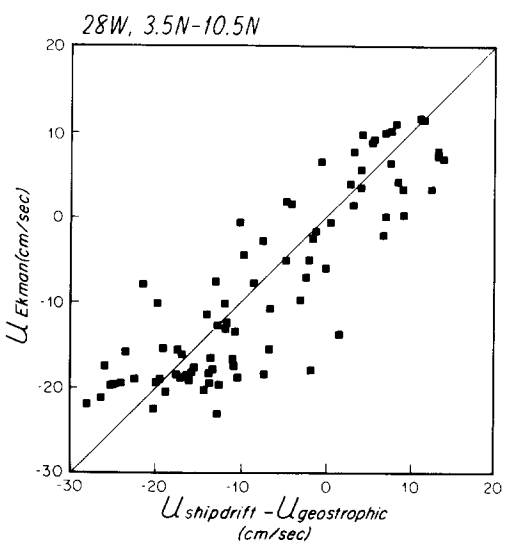

Fig. 3. Scatterplot of the eastward Ekman velocity from ARNAULT (1987) calculated using climatological wind stress (HELLERMAN and ROSENSTEIN, 1983) and the difference between the eastward velocity from historical ship drifts and the eastward geostrophic velocity derived from XBTs (see text). Values are monthly averages calculated for 1° latitude bins in the vicinity of the NECC near 28°W and extending from 3.5° to 10.5°N. The 45° line indicates a one to one correspondence between Ekman velocity and ship drift minus geostrophic velocity.

One of our main reservations about using the above technique to calculate surface gradients is that it incorporates any slippage that could be present in the historical ship drifts. We chose a vertical viscosity so that the calculated Ekman surface velocity matches the difference between ship drift velocity and geostrophic velocity. Later we add our calculated Ekman surface velocity to our calculated geostrophic velocity to estimate the total surface velocity. Thus any slippage in ship drifts would remain in our sum of Ekman plus geostrophic velocity.

Probably the best measurements of the wind-driven shear in the upper water column were reported by PRICE *et al.* (1987). In their study near 34°N, 70°W, current meter measurements revealed a mean current spiral with the 5 m current vector rotated about 80° to the right of the wind, and further clockwise rotation with depth being only 20° over an e-folding scale, or roughly one-third of the rotation expected in an Ekman spiral. The downwind velocity component at 5 m relative to that below the mixed layer was around 1 cm s^{-1}; the crosswind component was around 5 cm s^{-1}. PRICE *et al.* (1987) also use a numerical model of the ocean surface layer to simulate successfully the measured diurnal variability and mean current spiral. These values, especially the downwind component, are significantly smaller than the calculated Ekman surface velocity components of 9 cm s^{-1} (both downwind and crosswind) for 6°N using the HELLERMAN and ROSENSTEIN (1983) mean wind stress of 0.51 dyne cm^{-2} and A_z of 10^2 cm^2 s^{-1}. Compared to these model simulations, our calculated Ekman surface velocity is about two times too large and rotated too far downwind. PRICE *et al.* (1987) found that the surface velocity is nearly constant when the wind stress is varied by a factor of 4 (0.5–2.0 dyne cm^{-2}), but the surface velocity does vary significantly with variations in heat flux and Coriolis parameter. Using reasonable parameters for the NECC (τ of 0.5 dyne cm^{-2}, a net surface heat flux Q of 650 W m^{-2} at the daily maximum, and f corresponding to 6°N) their model predicts a downwind surface velocity (or, equivalently, shear over the mixed layer) of 3 cm s^{-1} and a crosswind velocity of 6 cm s^{-1} (PRICE, personal communication).

3. RESULTS AND DISCUSSION

3.1. *Geostrophic velocity*

The main pattern of dynamic height variations consists of a high of 87 dyn cm centered at 4.5°N in October and a low of 64 dyn cm centered at 11.5°N in September (Fig. 4a). The latitudinal gradient between the high and low is caused by the thermocline that slopes across the NECC. The slope is maximum in October and minimum in April due to seasonal variations in both the high and low regions, which are out of phase by approximately 180°. The pattern is very similar to a plot (Fig. 4b) of the annual variations of dynamic height given by inverted echo sounders and temperature records at 0°, 3°, 6°, 9°N, along 28°W: the maximum latitudinal gradient in dynamic height is observed at the same latitude, 7°–8°N, and the maximum difference in height across the NECC is around 20 dyn cm and occurs in September–October.

Geostrophic velocity in the seasonally averaged NECC is eastward year-round from 5° to 11°N (Fig. 4a, top panel). Maximum velocity is 30 cm s^{-1} at 7°N in October and minimum velocity is 6 cm s^{-1} at 7°N in April. The estimated errors due to seasonal variations of the T–S relation ($\sim$1 cm s^{-1}) and deep shear >400 m ($\sim$1 cm s^{-1}) are less than the 6 cm s^{-1} minimum. The complementary evidence from dynamic height and geostrophic velocity is that the NECC continues eastward throughout the year but is slowest in

April. This same conclusion was reached by REVERDIN *et al.* (1991) using similar data and by GARZOLI and RICHARDSON (1989) from inverted echo sounders and temperature records along 28°W.

The eastward volume transport of the NECC was estimated by summing the eastward velocity between 4.5° and 10.5°N. The average transport is 9×10^6 m^3 s^{-1}, maximum is 12×10^6 m^3 s^{-1} in October, and minimum is 5×10^6 m^3 s^{-1} in April (Fig. 5). Maximum transport per unit width is centered at 6°N. The transports are similar to the model simulations (figs 2 and 3: PHILANDER and PACANOWSKI, 1986) although the limits of the NECC are slightly different in the two calculations. The seasonal variation in transport is much less than the $\sim 30 \times 10^6$ m^3 s^{-1} calculated between 3° and 9°N at 28°W by GARZOLI and RICHARDSON (1989). The difference between the transports could be due to differences in measurement techniques and reference levels—two instruments at 3° and 9°N giving a time series along a single meridian vs zonal and seasonal averages of temperature sections.

The westward flowing geostrophic SEC has two maxima: 45 cm s^{-1} at 1°N in July, and 37 cm s^{-1} at 2°N in November. The geostrophic SEC appears to reverse briefly in April between 1° and 5°N. North of 10°N flow is very slow; maximum velocity is 2 cm s^{-1} westward near 14°N in September. No evidence is seen here for significant geostrophic flow in the NEC.

3.2. *Ekman surface velocity*

The principal winds are the Northeast Trades lying over the northern region and the Southeast Trades lying over the southern region (Fig. 6). These winds converge onto the Intertropical Convergence Zone, which migrates seasonally, starting near the equator in March, moving northward to lie over the mean position of the NECC in July, and then moving back down to the equator again. Near the center of the NECC, the winds are northeasterly during spring and southeasterly and southerly during summer and fall. The spring northeast winds have the largest stress around 0.7–0.8 dyne cm^{-2} (at 6°N, 28°W). The winds drive a westward Ekman surface current with a maximum of 24 cm s^{-1} centered near 11°N in January and an eastward current with a maximum of 11 cm s^{-1} centered near 5°N in August (Fig. 4). Near 7°N the Ekman velocity is eastward from July to October, adding to the geostrophic NECC, and westward the rest of the year, counter to the geostrophic NECC.

3.3. *Geostrophic plus Ekman velocity*

The geostrophic and Ekman zonal velocity components near the NECC add to give a maximum eastward velocity of 35 cm s^{-1} in September at 7°N (Fig. 4). They subtract to cause a reversal from February to May (near 7°N), with maximum westward velocity of 13 cm s^{-1} in April. These results suggest that the Northeast Trades drive a westward surface current which counters and overwhelms the weakened eastward geostrophic NECC. Thus the Northeast Trades are responsible for the reversal of the surface NECC. The magnitude of the reversal here is probably inflated by ship drift windage which will be discussed below.

The PRICE *et al.* (1987) model simulations of the mean Ekman surface velocity in the NECC suggest a westward component of only 6 cm s^{-1} (for northeast winds), which is

(a)

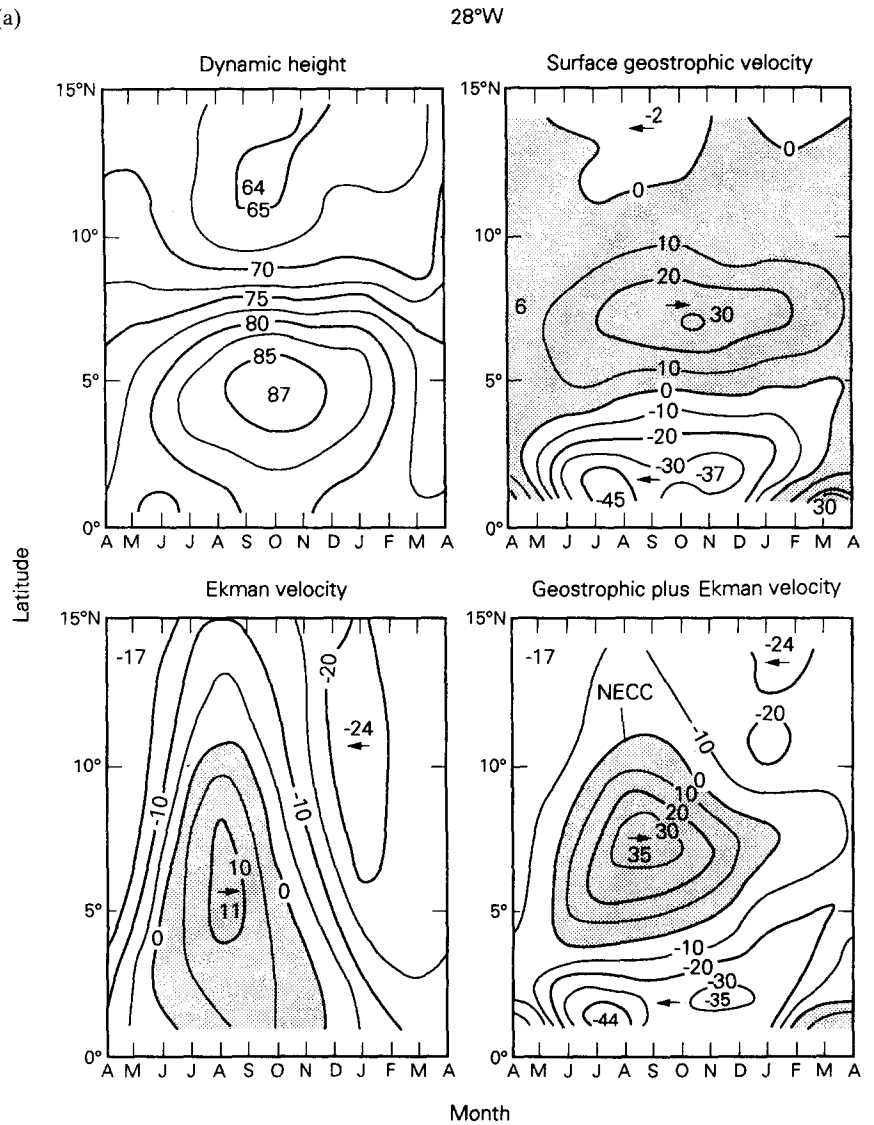

Fig. 4. (a) Time–latitude plots of dynamic height (in dyn cm relative to 440 m), of eastward component of surface geostrophic velocity (cm s^{-1}), of eastward Ekman surface velocity, and of the sum of geostrophic and Ekman velocity. Dynamic height was calculated from all available XBTs in vicinity of 28°W using salinity inferred from mean T–S curves. Geostrophic velocity was calculated from meridional gradients of dynamic height. Ekman velocity was calculated using monthly climatological wind stress values given by HELLERMAN and ROSENSTEIN (1983). The sum of geostrophic and Ekman velocities is a simple addition of the two fields. (b) Latitude–time plot of dynamic height from inverted echo sounders along 28°W at 0°, 3°, 9°N and from moored temperature recorders at 6°N (see GARZOLI and RICHARDSON, 1989). Travel times were converted to dynamic height by using hydrographic stations to calibrate the sounder data. The maximum meridional gradient which indicates the core of the NECC attained its northernmost position (north of 6°N) during the months of August–September and its southernmost position (south of 6°N) during March–April 1983 and in March 1984. This large scale latitudinal shifting of the NECC matches that of the Intertropical Convergence Zone.

(b)

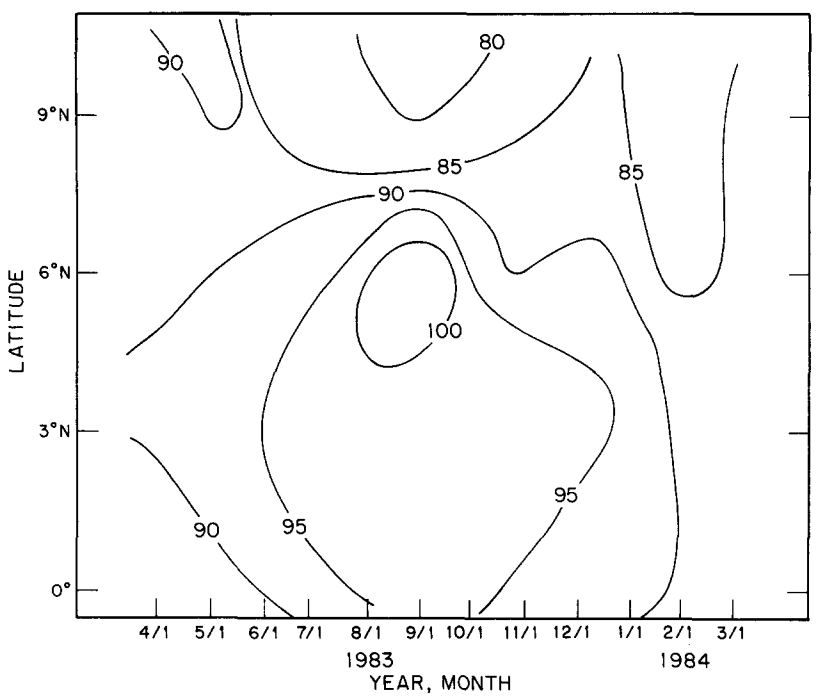

Fig. 4. *Continued.*

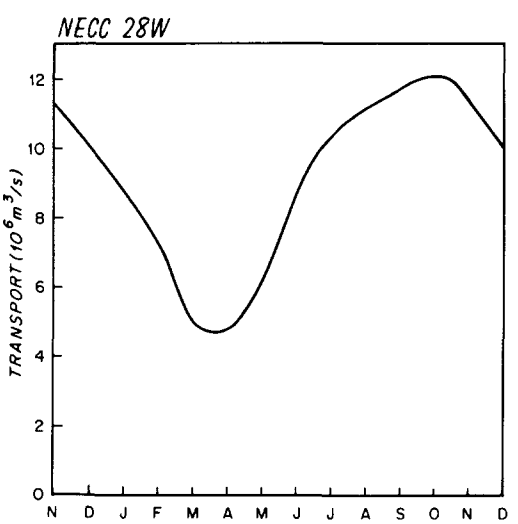

Fig. 5. Seasonal variation of the baroclinic transport of the NECC derived from the XBT data. Eastward transport was integrated in latitude from 4.5° to 10.5°N and in depth from the surface to 440 m.

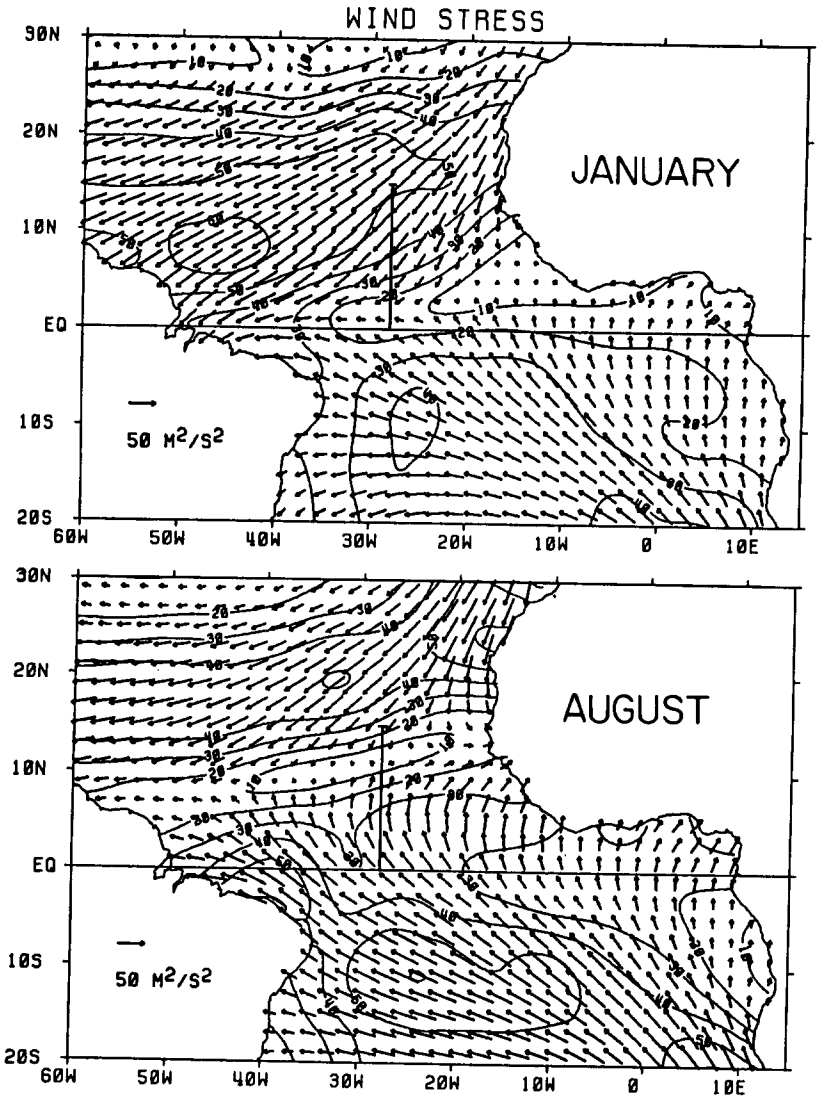

Fig. 6. Wind stress field for the tropical Atlantic showing values in January and August (SERVAIN *et al.*, 1987). The line along 28°W shows the region of the present study.

around the same magnitude as the eastward weakened geostrophic velocity in spring. Thus the model shear is not sufficient to cause much if any net westward velocity in the spring. However, it is possible that the strong Northeast Trades in spring ($\tau \sim 0.7$–0.8 dyne cm^{-2}) coupled with a large Q due to the sun's latitude overlying the NECC in spring combine to drive a swifter surface velocity than that simulated from mean conditions. If so, then an enhanced Ekman velocity would result in a net westward velocity as shown in Fig. 4.

The sum of the geostrophic and Ekman components also reveals a westward flowing SEC and NEC, with the NEC determined almost entirely by the Ekman component, and the SEC almost entirely by the geostrophic component.

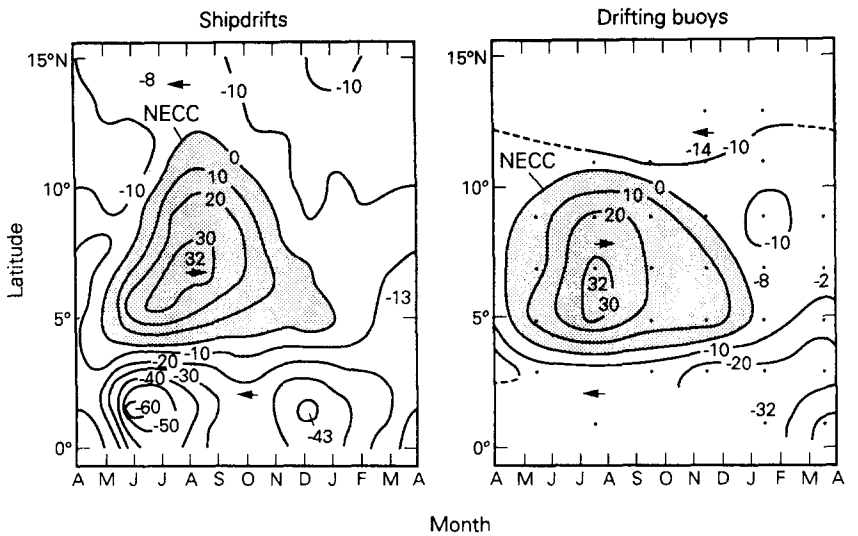

Fig. 7. Time–latitude plot of eastward velocity from historical ship drifts (1875–1976) and drifting buoys (1983–1985). The ship drift values were calculated and contoured on a 1° latitude by 1-month grid; drifting buoy velocities were grouped into bins 2° in latitude and 2 months in time as shown by dots. Values in boxes containing fewer than 10 observations were omitted.

3.4. *Ship drifts and drifters*

The combined Ekman and geostrophic velocity pattern is very similar to those from ship drifts and drifting buoys, although the buoy pattern is noisier and coarser due to the scarcity of data and larger boxes (Fig. 7). The similarity is not entirely surprising because the Ekman velocity was chosen to match the ship drift velocity minus the geostrophic velocity. The maximum velocities of the NECC determined by the three methods are almost exactly equal (32–35 cm s^{-1}) as is the timing of startup and decay. All three patterns have reversals of the NECC, with westward velocities of ~10 cm s^{-1}. Although the estimated standard error of a drifter's velocity is around 10 cm s^{-1}, large compared to the reversal velocity of ~8 cm s^{-1}, the rather smooth pattern of the seasonal variation and the consistent values at the time of the reversal suggest that the effect of random errors does not cause the reversal.

Ship drifts reveal the same two maxima in SEC velocities (July and December, near 1°–2°N), although the magnitudes are greater than Ekman plus geostrophic and there is a minimum but no reversal (as seen in February–April near 1°N). The ship drifts show that the peak velocity in the NECC meanders northward from about 5°N in May to 7°N in August and back to 5°N in December. The Ekman plus geostrophic velocity agrees with the first northward shift but not the southward return. That the three figures agree so well in general concerning the spatial and temporal velocity in the NECC suggests that the combined Ekman plus geostrophic velocity is quite realistic. Part of the similarity could be caused by systematic errors in ship drifts and drifters, errors that could also have been incorporated into the Ekman calculations of surface velocity.

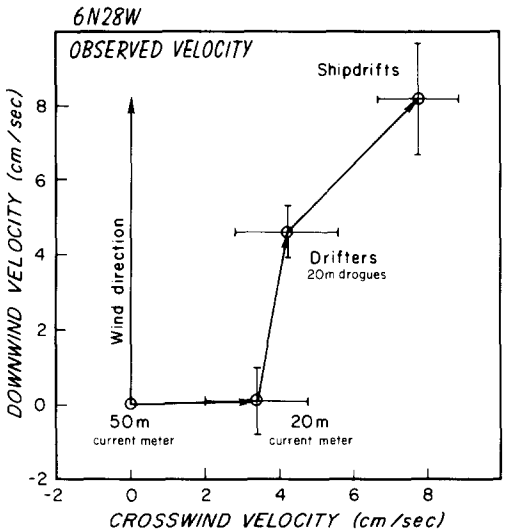

Fig. 8. Velocity shear in the upper 50 m measured between current meters at 50 and 20 m, between the 20 m current meter and drifters drogued at 20 m, and between the drifters and ship drifts. Crosswind and downwind components were calculated relative to the local wind direction (oriented northward here) and averaged coherently with respect to the wind. Standard errors are also shown (see Table 1). The crosswind velocity is interpreted to be a measure of shear in the mixed layer. The downwind velocity of the drifters and ship drifts is due to both shear and wind and wave induced slip.

3.5. *Discussion of systematic errors*

The velocity shear in the upper 50 m in the NECC was studied in order to reveal the details of the NECC reversal and to estimate the slippage of drifters and ship drifts. The velocity from current meters, drifters and ship drifts near 6°N, 28°W were averaged coherently with respect to the local wind direction (Figs 8 and 9, Table 1). If we assume that the velocity at 50 m is near the base of the mixed layer (the average difference in temperature between 50 and 20 m was only 0.7°C), then the shear above 50 m gives the local wind driven velocity. The velocity at 20 m relative to the velocity at 50 m determined from current meters is 3.4 cm s^{-1} and in a direction approximately 90° to the right of the wind direction. Relative to the 20 m current meter velocity, the velocity of the 20 m drogued drifters is primarily downwind at 4.5 cm s^{-1}. This velocity is interpreted to be downwind slippage of the drifters amounting to 0.68% of the wind speed and due to the force of the winds and waves on the buoy and floating part of the tether plus the force of the sheared velocity acting on the whole system.

The ship drift velocity (which is an average over the upper 5 m approximately) relative to the drifters is about 45° to the right of the wind at 5.0 cm s^{-1}. Part of the downwind velocity (3.6 cm s^{-1}) is due to slippage and part due to velocity shear. These results suggest that the drifters and ship drifts measured wind-driven velocity components (including slippage) approximately 45° to the right of the wind direction at 6.2 and 11.2 cm s^{-1}, respectively (Fig. 9). Both velocity vectors are in the same direction as the calculated Ekman velocity, and the ship drift value is nearly equal to it in magnitude (Fig. 9). This is another demonstration of why the velocity measured by ship drifts is so similar to that

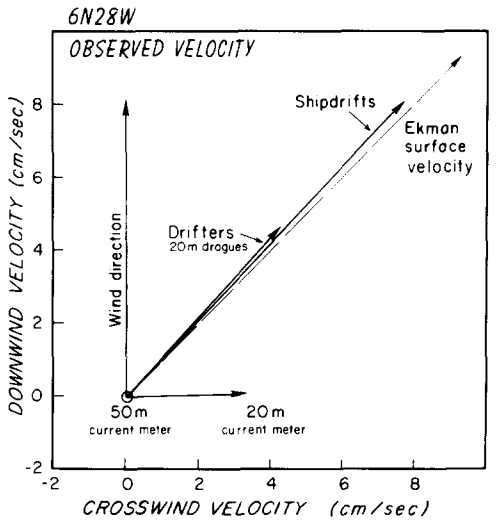

Fig. 9. Velocity shear in the upper 50 m as measured between a current meter centered at 50 m, and (1) a current meter at 20 m, (2) surface drifters with drogues centered at 20 m, and (3) historical ship drifts. Values were calculated relative to the local wind direction (see Fig. 8 and Table 1). The Ekman surface velocity $V_0 = \bar{\tau}/[\rho(A_z f)^{1/2}] = 13.1$ cm s^{-1} is also shown. V_0 was calculated using $\bar{\tau}$ the annual scalar average wind stress at 6°N, 28°W equal to 0.51 dyne cm^{-2} (HELLERMAN and ROSENSTEIN, 1983) and an assumed A_z equal to 10^2 cm^2 s^{-1}.

calculated by adding Ekman and geostrophic components—the wind driven component measured by ship drift is almost identical to the calculated Ekman velocity.

Two important questions which we now seek to answer are (1) what is the size of the systematic error in drifters and ship drifts and (2) are these sufficiently large to change the results? Specifically, is the downwind slippage large enough to cause the apparent reversal of the NECC in spring?

The average downwind slippage of drifters is estimated to be 4.5 cm s^{-1} (Table 1). This value of downwind slip agrees with the direct measurement of slip of various drogues by attached current meters (NIILER, personal communication). A relationship in which downwind slip is inversely proportional to R, slip $= 59/R$, accounts for 77% of this measured slip variance and suggests that a typical downwind slip for our buoys with $R = 16$ is 3.7 cm s^{-1} (NIILER, personal communication) which is reasonably close to the 4.5 cm s^{-1} $\pm$ 0.7 cm s^{-1} given in Table 1. A model which incorporates variations in both wind speed and shear (see CHERESKIN *et al.*, 1989) was fit to the observed slip data (NIILER, personal communication). Results suggest that the downwind slip correlated with wind speed is $\sqrt{2.1W^2/R}$, which equals 2.4 cm s^{-1} for our buoys, where W is wind speed, 6.6 m s^{-1} (Table 1), and the coefficient 2.1 was determined for holey sock drogues. The main point is that something like 50–60% of the downwind slip is due to windage; the rest is due to shear. The implication is that our drifters are slipping downwind at 4.5 cm s^{-1} with respect to the water at 20 m but less so with respect to surface water due to downwind shear. If the downwind shear is 3 cm s^{-1} [from the PRICE *et al.* (1987) model], then the downwind slip relative to surface water is only 1.5 cm s^{-1}. This issue is important when considering differences in velocity measured by drifters and ship drifts.

Table 1. *Observed shear in the upper* 50 m *near* 6°N, 28°W

Velocity observations	Downwind velocity (cm s^{-1})	Crosswind velocity (cm s^{-1})	Average wind stress (dyne cm^{-2})
(A) 20 m current meter–50 m current meter	0.1 ± 0.9	3.4 ± 1.4	0.33
(B) Drifters–20 m current meter	4.5 ± 0.7	0.8 ± 1.4	0.27
(C) Ship drifts–drifters	3.6 ± 1.5	3.5 ± 1.1	0.51

(A) Values are velocity shear calculated relative to the local wind direction and averaged coherently in time. Current meters recorded velocity at 6°N, 28°W for 392 days from February 1983 to March 1984 (RICHARDSON and REVERDIN, 1987). Downwind and crosswind velocity components were calculated relative to the local wind from the SEQUAL wind stress field each day and averaged over the whole record. Standard error was estimated from $\sqrt{2T\sigma/N}$ where σ is the velocity variance, N is the number of daily observations, and T is the integral time scale of the autocorrelation function (5.3 days for the crosswind direction and 2.3 days for downwind direction).

(B) Shear between drifters with drogues centered at 20 m and the 20 m current meter was determined from daily average velocities of 15 close passes (<30 km) of buoys to the current meter mooring. Wind direction was from a moored wind recorder at a height of 3 m for nine passes and from SEQUAL wind stress field for six passes. The estimated average wind speed for the 15 passes is 6.6 m s^{-1}. Standard error was estimated from the 15 shear values.

(C) Shear between ship drifts and drifters is from monthly averages of velocity calculated for boxes whose limits are 5°–9°N, 23°–33°W. Crosswind and downwind components of these are relative to monthly climatological wind stress given by HELLERMAN and ROSENSTEIN (1983) (which was greater than the 1983–1984 SEQUAL wind stress). On average there were 123 individual daily average drifter and 1026 ship drift observations per month. Standard error was estimated from the 12 monthly shear values.

The westward component of drifter slip for northeast winds in spring is estimated to be 2–3 cm s^{-1} depending on whether we use just the part correlated with wind speed or the total downwind slip. In either case the size of this systematic wind induced error is less than the average 6–8 cm s^{-1} westward velocity in the NECC observed by drifters in January and February. Thus we conclude that systematic errors are not so large as to cause the observed westward reversal of the NECC. Note that the winds are primarily southerly during the summer maximum of the NECC (Fig. 6); thus the zonal component of wind induced slip will be small at that time.

Relative to the 50 m level, the mean ship drift velocity is 8.2 cm s^{-1} downwind and 7.7 cm s^{-1} crosswind (Table 1). The model simulated shear values of 3 cm s^{-1} downwind and 6 cm s^{-1} crosswind imply that the downwind ship-drift slip is around 5 cm s^{-1}. Note that the crosswind component of ship drift, 7.7 ± 2.3 cm s^{-1}, is not significantly different from the model's value. The westward component of ship-drift slip for northeast wind is 4–6 cm s^{-1} depending on whether all the relative downwind ship-drift velocity is used or only the part left over after the simulated shear is subtracted. This systematic error is around half the westward ship-drift velocities of ~10 cm s^{-1} observed in the NECC during March and April. Thus, as in the case for drifters, the systematic errors are smaller than the observed westward reversal in the NECC. However, it is possible that the larger than average wind stress in spring (~0.7–0.8 dyne cm^{-2}) could generate a larger than average downwind slip for both drifters and ships which might approach the magnitude of the observed westward velocity.

This discussion of estimated wind driven shears and slip leaves unanswered a nagging discrepancy. Although both drifters and ship drifts agree in showing westward currents of

4–5 cm s^{-1} in the NECC during spring, the westward drifter velocity peaks at 8 cm s^{-1} in January and February at the same time that the geostrophic NECC is eastward at ~20 cm s^{-1} (7°–8°N). The shear calculations (Table 1) plus the PRICE *et al.* (1987) current meter results and model simulations suggest a westward wind driven shear of ~6 cm s^{-1}, not enough to reverse such a large geostrophic velocity. A possible explanation of this discrepancy concerns the different years during which the data sets were measured. Phase shifts in timing of the average seasonal cycle of currents observed in the different data could appear as large velocity discrepancies for a particular month. It is also possible that the real wind driven near surface velocity plus slip is larger than that estimated above for mean conditions. Clearly a better set of velocity data in the mixed layer is needed to sort out these issues.

Acknowledgements—Funds were provided by National Science Foundation grants OCE89-22833 and OCE89-15926. G. Heimerdinger helped us obtain the XBT data, and J. Price provided results from his numerical model. C. Wooding and L. Hale calculated and plotted the results, R. Davis drafted the figures, and M. A. Lucas typed the manuscript. J. Price and S. Wacongne critically reviewed an earlier version of this paper. Woods Hole Oceanographic Institution Contribution No. 6972.

REFERENCES

ARNAULT S. (1987) Tropical Atlantic geostrophic currents and ship drifts. *Journal of Geophysical Research*, **92**, 5076–5088.

BRUCE J. G. (1987) XBT observations between 10°N–10°S in the Atlantic from ships-of-opportunity, complemented by AXBT surveys. Woods Hole Oceanographic Institution Technical Report, WHOI-87-41.

CHERESKIN T. K., P. P. NIILER and P.-M. POULIN (1989) A numerical study of the effect of upper ocean shear on flexible drogued drifters. *Journal of Atmospheric and Oceanic Technology*, **6**, 243–253.

COCHRANE J. D., F. J. KELLEY JR and C. R. OLLING (1979) Subthermocline countercurrents in the western equatorial Atlantic Ocean. *Journal of Physical Oceanography*, **9**, 724–738.

EMERY W. J., W. ZENK, K. HUBER, P. RUAL and P. NOWLAN (1987) Trends in Atlantic equatorial current variability. *Deutsche Hydrographische Zeitschrift*, **40**, 261–276.

GARZOLI S. L. and E. J. KATZ (1983) The forced annual reversal of the Atlantic North Equatorial Countercurrent. *Journal of Physical Oceanography*, **13**, 2082–2090.

GARZOLI S. L. and P. L. RICHARDSON (1989) Low frequency meandering of the North Equatorial Countercurrent. *Journal of Geophysical Research*, **94**, 2079–2090.

HALPERN D. (1979) Observations of upper ocean currents at dome sites A, B, and C in the tropical central North Pacific Ocean during 1975 and 1976. In: *Marine geology and oceanography of the Pacific manganese nodule province*, J. L. BISCHOFF and D. Z. PIPER, editors, Plenum Publishing Corporation, pp. 43–82.

HEIMERDINGER G. (1987) Inventory of oceanographic data, equatorial Atlantic 1980–1984, a SEQUAL working document prepared by the SEQUAL data management office, Woods Hole Oceanographic Institution, Woods Hole, MA.

HELLERMAN S. and M. ROSENSTEIN (1983) Normal monthly wind stress over the world ocean with error estimates. *Journal of Physical Oceanography*, **13**, 1093–1104.

HENIN C. and P. HISARD (1987) The North Equatorial Countercurrent (NECC) observed during FOCAL. *Journal of Geophysical Research*, **92**, 3751–3758.

KATZ E. (1987) Seasonal response of the sea surface to the wind in the equatorial Atlantic. *Journal of Geophysical Research*, **92**, 1885–1893.

MCPHADEN M. J., D. V. HANSEN and P. L. RICHARDSON (1991) A comparison of ship drift, drifting buoys and current meter mooring velocities in the Pacific South Equatorial Current. *Journal of Geophysical Research*, **96**, 775–781.

MELE P. A. and E. J. KATZ (1985) Report of XBT data from four SEQUAL cruises. Report No. LDGO-85-2 from Lamont–Doherty Geological Observatory.

MERLE J. and S. ARNAULT (1985) Seasonal variability of the surface dynamic topography in the tropical Atlantic Ocean. *Journal of Marine Research*, **43**, 267–288.

PERKINS H. T. and K. D. SAUNDERS (1984) Atlantic equatorial sections during July 1983. *Geophysical Research Letters*, **11**, 769–772.

PHILANDER S. G. H. and R. C. PACANOWSKI (1986) The mass and heat budget in a model of the tropical Atlantic ocean. *Journal of Geophysical Research*, **91**, 14,212–14,220.

PRICE J. F., R. A. WELLER and R. R. SCHUDLICH (1987) Wind-driven ocean currents and Ekman transport. *Science*, **238**, 1534–1538.

REVERDIN G., P. RUAL, Y. DUPENHOAT and Y. GOURIOU (1991) Vertical structure of the seasonal cycle in the central equatorial Atlantic Ocean: XBT sections from 1980 to 1988. *Journal of Physical Oceanography*, **21**, 277–291.

RICHARDSON P. L. and T. K. MCKEE (1984) Average seasonal variation of the Atlantic Equatorial currents from historical ship drifts. *Journal of Physical Oceanography*, **14**, 1226–1238.

RICHARDSON P. L. and G. REVERDIN (1987) Seasonal cycle of velocity in the Atlantic North Equatorial Countercurrent as measured by surface drifters, current meters, and ship drifts. *Journal of Geophysical Research*, **92**, 3691–3708.

RICHARDSON P. L. and D. WALSH (1986) Mapping climatological seasonal variations of surface currents in the tropical Atlantic using ship drifts. *Journal of Geophysical Research*, **91**, 10,537–10,550.

RUAL P. and F. JARRIGE (1984) Tropical Atlantic thermal structures along the Europe–Brazil ship line. *Geophysical Research Letters*, **11**, 775–778.

SERVAIN J., M. SEVA, S. LUKAS and G. ROUGIER (1987) Climatic atlas of the tropical Atlantic wind stress and sea surface temperature: 1980–1984. *Ocean–Air Interactions*, **1**, 109–182.